The Astronomical Journal, 149:134 (8pp), 2015 April doi:10.1088/0004-6256/149/4/134

ARCHIVAL OBSERVATIONS OF ACTIVE ASTEROID 313P/GIBBS

Man-To Hui[1] and David Jewitt[1,2]
[1] Department of Earth, Planetary and Space Sciences, UCLA, 595 Charles Young Drive East, Los Angeles, CA 90095-1567, USA; pachacoti@ucla.edu
[2] Department of Physics and Astronomy, UCLA, 430 Portola Plaza, Box 951547, Los Angeles, CA 90095-1547, USA
Received 2015 January 6; accepted 2015 February 9; published 2015 March 16

ABSTRACT

We present prediscovery observations of active asteroid 313P/(2014 S4) Gibbs taken in 2003 and 2004. Sloan Digital Sky Survey observations from 2003 establish that, after 133P/Elst–Pizarro and 238P/Read, 313P is only the third main-belt active asteroid to show mass loss in different orbits. This repetitive activity is consistent with mass loss driven by the sublimation of ice. A Finson-Probstein model is used to analyze the morphology of the object, showing that the activity was continuous but declining steadily over two months of observation in 2003. Ejected dust particles are dominated by relatively large sizes with radii from ~25 to ~600 μm. We estimate from photometry the dust mass loss rate to be $\lesssim$0.2 kg s^{-1}. In contrast, Subaru telescope observations from 2004 show no evidence for mass loss and suggest a bare nucleus. The color, nucleus size, and the mass loss rates of 313P measured in 2003 are consistent with published values obtained from data taken in 2014. However, the effective cross-section was larger than in 2014 by a factor of ~2, indicating a decline in the activity between orbits. A new orbital solution gives a 5σ upper limit to the transverse non-gravitational parameter $\mathfrak{A}_2 \lesssim 2.45 \times 10^{-8}$ AU day^{-2}.

Key words: comets: general – minor planets, asteroids: general – minor planets, asteroids: individual (313P/2014 S4 Gibbs)

1. INTRODUCTION

313P/(2014 S4) Gibbs (hereafter called 313P) was discovered on 2014 September 24 in the course of the Catalina Sky Survey (Gibbs 2014). The orbit has semimajor axis $a = 3.156$ AU, eccentricity $e = 0.242$, and inclination $i = 11\overset{\circ}{.}0$, classifying 313P as a new member of the active asteroid (a.k.a. main-belt comet) population.

A great diversity of mechanisms can cause mass loss from asteroids, including sublimation, thermal fracture, rotational instability, and impact (Jewitt 2012). Jewitt et al. (2014) analyzed post-discovery observations of 313P and concluded that the properties of this object are consistent with the sublimation of near-surface ice. Here, we analyze archival observations of 313P and use these observations to further constrain the nature and origin of its activity.

2. OBSERVATIONS

We used the Solar System Object Image Search facility of the Canadian Astronomical Data Centre[3] (CADC) (Gwyn et al. 2012) to search for archival observations of 313P at positions based upon ephemerides provided by JPL Horizons and the Minor Planet Center (MPC). After visually scrutinizing the images, we identified the object in Sloan Digital Sky Survey (SDSS) 2.5 m telescope data from 2003 and in Suprime-Cam CCD (Miyazaki et al. 2002) images from the 8 m Subaru telescope from 2004. The SDSS, observing 313P on 5 separate days between 2003 September and November, employed standard Sloan *ugriz* filters, thereby providing a valuable opportunity to study the object at several wavelengths. Each day included only one observation through each filter. Archival Sloan images are fully corrected for bias and flat field systematics. The data have an image scale 0.″40 pixel^{-1}, while typical image quality is ~1.″0 FWHM. The exposures through each filter were all of 54 s duration.

Subaru observations were identified on two days in 2004 September, both through a broadband VR filter. Exposures were all 60 s in duration, the images have a pixel scale of 0.″20 pixel^{-1}, and seeing was ~0.″9 (FWHM) on both days. The downloaded Subaru images were raw, and therefore we performed standard image calibration using bias and flat field frames obtained from the Subaru Mitaka Okayama Kiso Archive System[4] (SMOKA) before conducting measurements.

The CADC also revealed *Wide-field Infrared Survey Explorer* thermal observations from 2010 March. However, nothing was detected around the predicted positions according to the ephemerides computed by JPL Horizons, presumably due to the faintness of the object.

Table 1 lists the observational geometry of the SDSS and Subaru observations.

3. RESULTS

3.1. Morphology

We analyzed the morphology of 313P in all the SDSS and Subaru archival data. Sample images are presented in Figure 1 in chronological order. We think that the change in morphology in 2003 is largely due to the changing observational geometry, rather than to intrinsic variations in its activity. The Subaru data from 2004, in contrast, show a completely stellar appearance, with a FWHM ~0.″9 that is the same as nearby stars of similar brightness.

We employed a syndyne and synchrone model (Finson & Probstein 1968) to study the morphology of 313P. The trajectories of dust grains with respect to the parent nucleus are determined by the ratio of the solar radiation force on the grain to the gravitational force due to the Sun, denoted as β, by the initial ejection velocity, as well as by the time they are released. The quantity β is inversely proportional to the product of the grain radius, a, with the dust density, ρ_d, which

[3] http://www2.cadc-ccda.hia-iha.nrc-cnrc.gc.ca/en/

[4] http://smoka.nao.ac.jp

Table 1
Observational Geometry

Date (UT)	Tel[a]	r_h[b]	Δ[c]	α[d]	θ[e]	PsAng[f]	PsAMV[g]
2003 Sep 30.396	SDSS	2.434	1.598	16.1	30.5	272.8	246.1
2003 Oct 23.345	SDSS	2.465	1.512	8.5	37.0	303.3	246.7
2003 Oct 24.346	SDSS	2.467	1.511	8.2	37.3	305.9	246.8
2003 Nov 20.252	SDSS	2.510	1.580	9.6	44.6	35.5	247.7
2003 Nov 28.240	SDSS	2.525	1.636	12.1	46.8	47.0	247.8
2004 Sep 15.620	SUPA	3.205	3.751	14.0	108.5	283.5	271.2
2004 Sep 16.623	SUPA	3.208	3.742	14.1	108.7	283.6	271.3

Notes.
[a] Telescope: SDSS = SDSS 2.5 m; SUPA = Subaru 8 m.
[b] Heliocentric distance, in AU.
[c] Cometocentric distance to the observatory, in AU.
[d] Phase angle, in degrees.
[e] True anomaly, in degrees.
[f] Position angle of the extended Sun-to-313P radius vector in the plane of sky, in degrees.
[g] Position angle of the projected negative heliocentric velocity vector, in degrees.

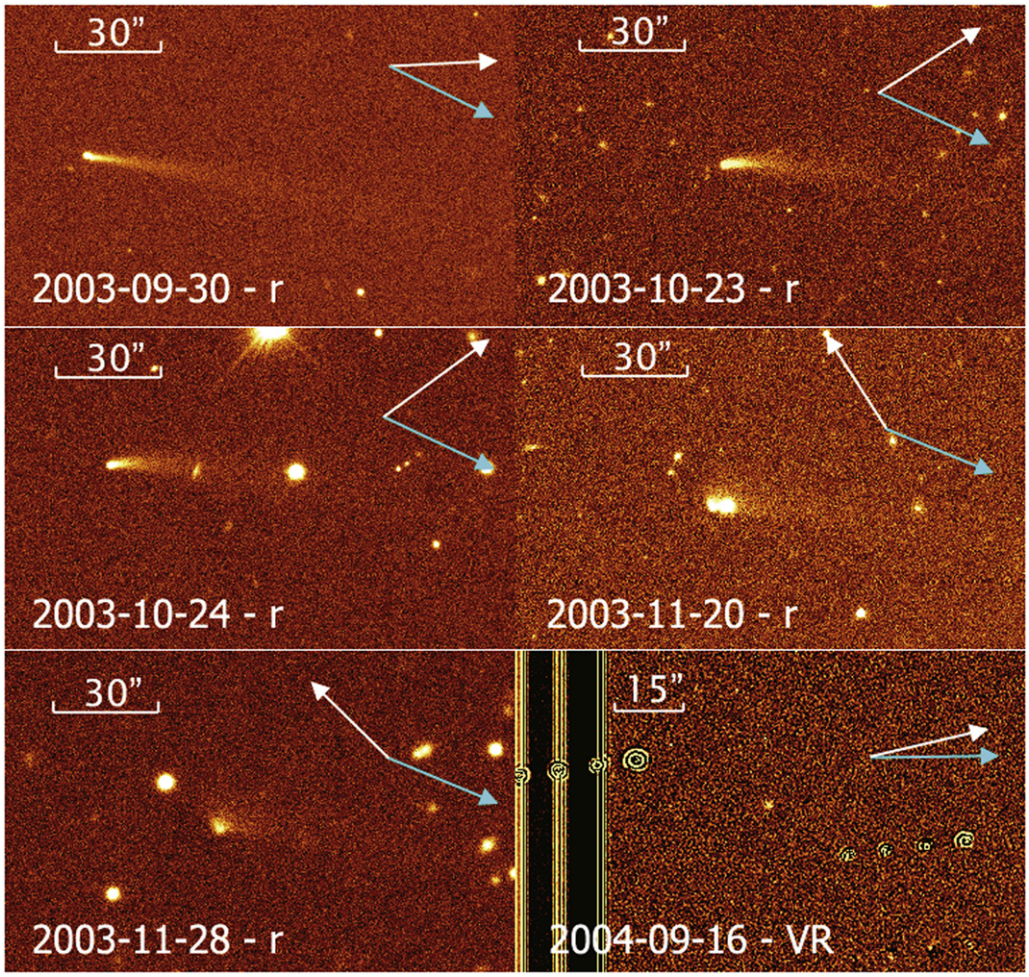

Figure 1. Archival SDSS and Subaru images of 313P with dates and filters labeled. In each panel, north is to the top and east to the left. The cyan arrows point to the projected negative heliocentric velocity vector, and the white arrows point to the projected anti-solar direction.

means that the size of the dust particles can be estimated from the corresponding β value given that ρ_d is assumed (c.f. Bohren & Huffman 1983; Fulle 2004). In the Finson-Probstein model, the ejection velocity is assumed to be zero with respect to the nucleus. The loci of positions of particles driven by the same β, but released at different times, are called syndynes. The loci of positions of particles released at the same time, but driven by different β, are called synchrones. While the zero velocity approximation may not be particularly realistic for 313P, it is clear from Figure 2 that the morphology in 2003 was better matched by syndynes than by synchrones. We conclude that the activity of 313P is more nearly continuous than impulsive, at least around the 2003 September–November period.

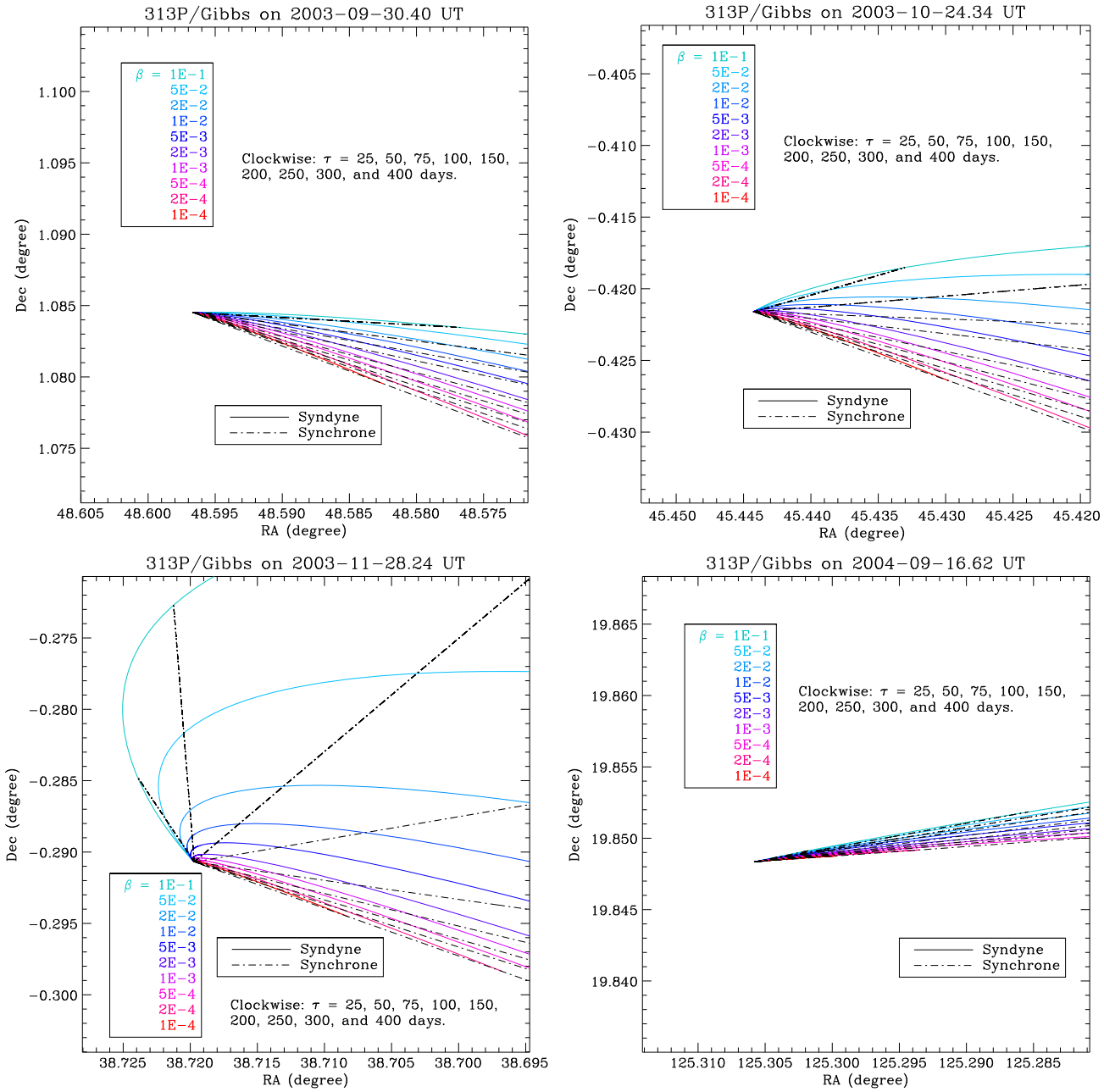

Figure 2. Syndyne and synchrone lines corresponding to the upper and lower panels of Figure 1. Syndynes are depicted as solid lines in colors, whereas synchrones are drawn as dashed lines in black. North to the top and east to the left. Both the R.A. and decl. are expressed in degrees.

In observations from 2003 September to October, the tail appeared narrow and thin. An improved viewing geometry in 2003 November revealed a fan-shaped tail morphology, providing better separation of dust particle trajectories by their β values. From a comparison between the simulations and observations, we conclude that syndynes with $\beta \sim 5 \times 10^{-2}$ to 2×10^{-3} can describe the tail very well. If a typical $\rho_d = 1\,\mathrm{g\,cm^{-3}}$ is assumed, we find grain radii $a \sim 25$ –600 μm. These grains are relatively large compared to those found in typical active comets (Fulle 1999). However, comparably large grains were inferred from syndyne-synchrone analysis in data from 2014 (Jewitt et al. 2015; Hsieh et al. 2015). Active asteroid 133P/Elst–Pizarro, itself thought to be sublimation-driven, also shows large dust grains (Hsieh et al. 2004; Jewitt et al. 2014).

3.2. Photometry

We used circular apertures to measure the apparent magnitudes of 313P. The SDSS images from 2003 November 20 were discarded because of field star contamination (see Figure 1). The SDSS images were measured separately, but the Subaru images were digitally co-added before measurement in order to increase the signal-to-noise ratio (S/N) of the data and to eliminate background objects. For this purpose, we used optimal subtraction with a spatially variable kernel to the images in ISIS2.2[5] (Alard 2000). We then stacked the images, both aligned on the field stars and registered to the motion of 313P according to the value provided by JPL Horizons

[5] http://www2.iap.fr/users/alard/package.html

Table 2
Photometry of 313P/Gibbs

Date (UT)	Filter	m_λ (AB System)	m_λ (Vega System)	$A_\lambda(\alpha)f\rho$ (cm)	$A_\lambda(0°)f\rho$ (cm)	C_e (km^2)
2003 Sep 30	u	20.80 ± 0.28	19.83 ± 0.28	...	...	...
2003 Sep 30	g	19.12 ± 0.07	19.22 ± 0.07	16.6 ± 1.2	22.0 ± 1.6	17.3 ± 1.3
2003 Sep 30	r	18.57 ± 0.08	18.41 ± 0.08	17.7 ± 1.3	23.4 ± 1.8	18.4 ± 1.4
2003 Sep 30	i	18.39 ± 0.08	18.00 ± 0.08	19.5 ± 1.5	25.8 ± 2.0	20.3 ± 1.5
2003 Sep 30	z	18.44 ± 0.12	17.88 ± 0.12	18.3 ± 2.0	24.2 ± 2.7	19.0 ± 2.1
2003 Oct 23	u	20.20 ± 0.15	19.24 ± 0.15	...	...	...
2003 Oct 23	g	18.97 ± 0.08	19.07 ± 0.08	17.5 ± 1.3	19.2 ± 1.5	15.1 ± 1.3
2003 Oct 23	r	18.42 ± 0.08	18.25 ± 0.08	18.7 ± 1.5	20.5 ± 1.6	16.1 ± 1.5
2003 Oct 23	i	18.28 ± 0.08	17.89 ± 0.08	19.8 ± 1.6	21.7 ± 1.7	17.0 ± 1.6
2003 Oct 23	z	18.23 ± 0.12	17.67 ± 0.12	20.4 ± 2.3	22.4 ± 2.6	17.6 ± 2.2
2003 Oct 24	u	20.34 ± 0.14	19.38 ± 0.14	...	...	...
2003 Oct 24	g	19.00 ± 0.07	19.10 ± 0.07	16.9 ± 1.2	18.4 ± 1.3	14.5 ± 1.3
2003 Oct 24	r	18.50 ± 0.08	18.33 ± 0.08	17.3 ± 1.3	18.9 ± 1.4	14.8 ± 1.4
2003 Oct 24	i	18.31 ± 0.08	17.92 ± 0.08	19.3 ± 1.5	21.0 ± 1.6	16.5 ± 1.6
2003 Oct 24	z	18.30 ± 0.12	17.74 ± 0.12	19.1 ± 2.2	20.8 ± 2.4	16.3 ± 2.2
2003 Nov 28	u	20.73 ± 0.20	19.76 ± 0.20	...	...	...
2003 Nov 28	g	19.44 ± 0.08	19.54 ± 0.08	13.8 ± 1.0	16.5 ± 1.2	12.9 ± 1.3
2003 Nov 28	r	18.88 ± 0.08	18.72 ± 0.08	15.0 ± 1.2	17.8 ± 1.4	14.0 ± 1.5
2003 Nov 28	i	18.71 ± 0.08	18.32 ± 0.08	16.4 ± 1.2	19.5 ± 1.5	15.3 ± 1.5
2003 Nov 28	z	18.83 ± 0.13	18.27 ± 0.13	14.5 ± 1.8	17.2 ± 2.1	13.5 ± 2.3
2004 Sep 15	VR	24.10 ± 0.19	23.93 ± 0.19	1.0 ± 0.2	1.3 ± 0.2	1.0 ± 0.2
2004 Sep 16	VR	24.03 ± 0.16	23.87 ± 0.16	1.1 ± 0.2	1.4 ± 0.2	1.1 ± 0.2

Note. The measurements employed a fixed circular aperture of radius $\rho = 5000$ km. Apparent magnitudes of 313P in the AB and Vega system are both shown. See Figures 3 and 4 for a better illustration.

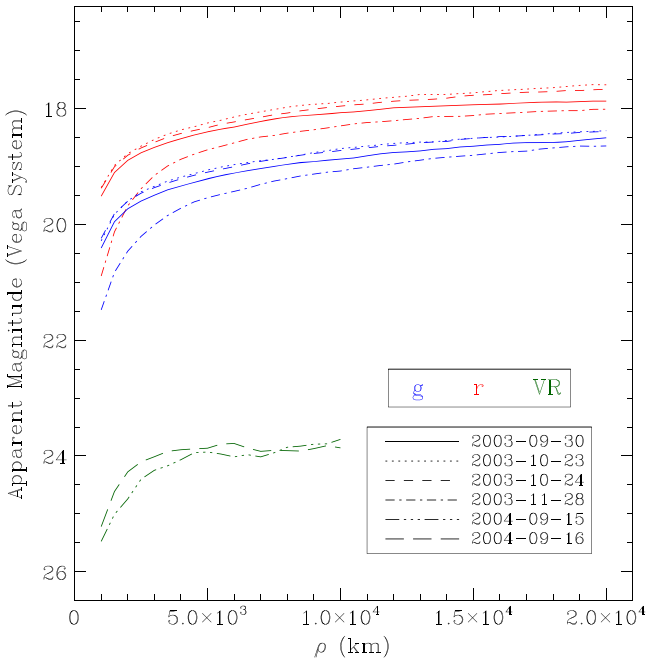

Figure 3. Apparent magnitudes in the Vega system as a function of the radial distance ρ to the optocenter of 313P. Only g-band, r-band, and the Subaru data are plotted. Data in i- and z-band filters show similar trends, while u-band data have large uncertainty and are not plotted.

software. The resulting images show a clean background around the object free from field star contamination and suitable for aperture photometry.

Zero-points of the SDSS images and stacked Subaru images (aligned on field stars) were determined with the

Table 3
Apparent Magnitudes of the Sun in the SDSS *ugriz* System

Band	$m_{\odot,\lambda}$ (AB System)	$m_{\odot,\lambda}$ (Vega System)
u	−25.10	−26.08
g	−26.42	−26.32
r	−26.89	−27.06
i	−26.97	−27.35
z	−26.99	−27.55

Note. Computation method of deriving the apparent magnitudes is described in Section 3.2. The error in each band is estimated to be $\sim \pm 0.03$.

Ninth Data Release (DR9) of the SDSS (Ahn et al. 2012) in the VizieR Service. The VR filter at Subaru is not a standard photometric filter, but has a bandpass similar to that of the Sloan r filter. Specifically, the VR filter has 50% transmission at wavelengths $\lambda \sim 5000$ and ~7000 Å (Jewitt et al. 1996), while the Sloan r 50% transmission wavelengths are at ~5500 and ~7000 Å. Both filter transmissions are approximately flat-topped. We therefore calibrated the VR filter to the Sloan r expecting that the resulting systematic error in the calibration is smaller than the statistical uncertainty due to the low S/N of 313P in the data. The zero-points were all in the AB system at this stage. Then, we measured the SDSS photometry of 313P within a series of circular apertures having fixed linear radii from $\rho = 1000$ to 20,000 km, with a radius increment of 500 km. In the Subaru data, the maximum linear radius was limited to 10,000 km to reduce uncertainties in the subtracted background to an acceptable level. We first

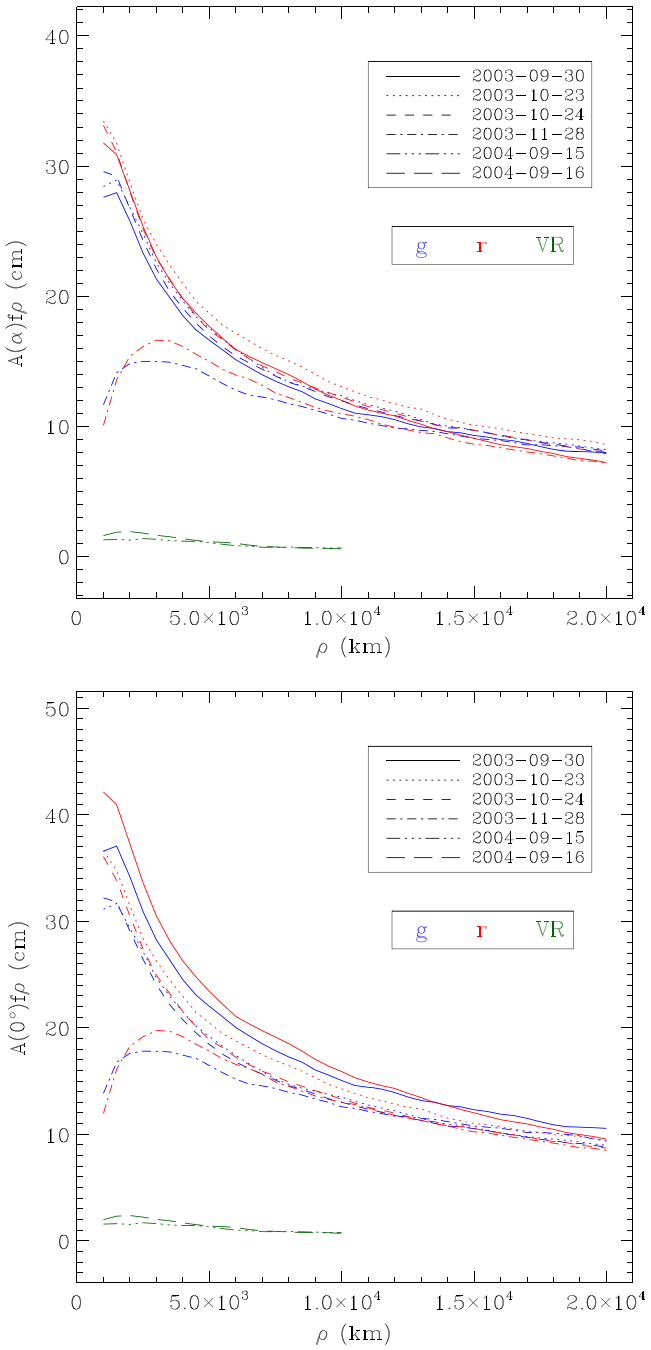

Figure 4. $Af\rho$ as a function of ρ calculated from g-, r-band, and Subaru data only. The lower panel is the same as the upper panel but includes phase effect corrections. The i- and z-band data show similar trends but are not plotted in the interests of clarity.

converted the apparent AB magnitudes of 313P from fluxes according to the corresponding zero-point values. The relationships between magnitudes in the AB and Vega systems listed in the table at http://www2.cadc-ccda.hia-iha.nrc-cnrc.gc.ca/en/megapipe/docs/filt.html were applied to obtain the magnitudes in the Vega system. We use the Vega system magnitudes in the following paragraphs unless otherwise noted. Uncertainties of the magnitudes were estimated from the errors in the zero-points and from statistical uncertainty in the CCD detector counts.

We studied the color of 313P by choosing $\rho = 5000$ km as standard aperture radius that is large enough to enclose the majority of the coma. There are 4 measurements in total in each band. The resulting mean values are $u - g = 0.32 \pm 0.20$, $g - r = 0.80 \pm 0.03$, $r - i = 0.39 \pm 0.02$, and $i - z = 0.15 \pm 0.07$ in the Vega system (Table 2), and the listed uncertainties are the standard deviations on the means of the measured values. The large uncertainty of the $u - g$ color index is due to the extremely poor S/N of the target in u-band images, and thus we discarded those data in the following analysis. As a comparison, the Sun has $(g - r)_\odot = 0.74$, $(r - i)_\odot = 0.29$, and $(i - z)_\odot = 0.20$ (see Table 3), thereby indicating a color slightly redder than the Sun. In order to compare our results to the color indices found by Jewitt et al. (2015), we transformed the color from the *ugriz* system to the *UBVRI* system. The AB magnitude data were fed into the conversion equations between *ugriz* and *UBVRI* (Jester et al. 2005) to yield the color of 313P in the *UBVRI* system. We obtained $B - V = 0.75 \pm 0.04$ and $V - R = 0.41 \pm 0.03$, in agreement with the measurements of $B - V = 0.72 \pm 0.02$, $V - R = 0.38 \pm 0.03$ in data from 2014 (Jewitt et al. 2015).

We also calculated the $A_\lambda(\alpha)f\rho$ (A'Hearn et al. 1984) by

$$A_\lambda(\alpha)f\rho = 4\frac{(\Delta r_h)^2}{\rho}10^{0.4(m_{\odot,\lambda}-m_\lambda)} \quad (1)$$

where A_λ is the albedo as a function of phase angle α, f is the filling factor, r_h is the heliocentric distance of 313P, Δ is the distance between 313P and the corresponding observatory, m_λ is the apparent magnitude of 313P, and $m_{\odot,\lambda}$ is the apparent magnitude of the Sun at wavelength λ. Equation (1) gives a measure of the quantity of dust within the projected photometry aperture. We were not aware of any precise *ugriz* magnitudes of the Sun in the Vega system. Instead of employing conversion formulae between the *u'g'r'i'z'* and *ugriz* systems[6] for fear of introducing extra relatively large uncertainties caused by stars of different colors, we directly computed the convolution of the solar spectrum[7] and the response functions of SDSS 2.5 m *ugriz* filters (Doi et al. 2010) to derive the flux of the Sun in the *ugriz* system. We estimated an error of $\sim \pm 0.03$ mag in the magnitudes of the Sun in the *ugriz* system, which we took into consideration and propagated to the uncertainties of the $A_\lambda f\rho$. The magnitudes of the Sun we computed are summarized in Table 3.

3.3. Search for Non-gravitational Acceleration

We used Astrometrica[8] to measure astrometry of 313P, rejecting SDSS observations from November 20 through Sloan z and g because of blending with a field star. The USNO-B 1.0 Catalog (Monet et al. 2003) was used to solve the plate constants up to the fourth order using $\gtrsim$30 reference stars in the u-band images (in which suitable stars are rare) to $\gtrsim$100 stars in other data. Resulting centroiding errors are $\sim \pm 0\farcs1$ to $\sim \pm 0\farcs3$. The positions of 313P in SDSS data from 2003 are close to the ephemeris predictions from JPL Horizons software to within $\sim 1''$ However, the positions measured from Subaru

[6] http://classic.sdss.org/dr7/algorithms/jeg_photometric_eq_dr1.html
[7] We used the 1985 Wehrli Standard Extraterrestrial Solar Irradiance Spectrum, available at http://rredc.nrel.gov/solar/spectra/am0/wehrli1985.new.html.
[8] http://www.astrometrica.at

Table 4
Derived Orbital Elements (Reference: Heliocentric Ecliptic J2000.0)

Element	Value without $\mathfrak{A}_2$	1σ Uncertainty	Value with $\mathfrak{A}_2$	1σ Uncertainty	Units
P[a]	5.58328	1.4×10^{-6}	5.58297	8.5×10^{-5}	yr
a[b]	3.14717325	5.3×10^{-7}	3.14705827	3.2×10^{-5}	AU
e[c]	0.24798776	6.3×10^{-6}	0.24795216	1.2×10^{-5}	...
i[d]	10.96271330	5.6×10^{-5}	10.96288637	7.3×10^{-5}	deg
Ω[e]	106.69129114	3.6×10^{-4}	106.69055335	4.1×10^{-4}	deg
ω[f]	253.49493781	1.1×10^{-3}	253.49309839	1.2×10^{-3}	deg
M_0[g]	18.14704320	2.9×10^{-4}	18.15031749	9.5×10^{-4}	deg
$\mathfrak{A}_2$[h]	...	...	1.77×10^{-8}	4.9×10^{-9}	AU day^{-2}

Notes. The rms of the pure-gravity orbital solution is $\pm 0\farcs577$ and of the solution including $\mathfrak{A}_2$ is $\pm 0\farcs524$.
[a] Orbital period.
[b] Semimajor axis.
[c] Eccentricity.
[d] Inclination.
[e] Longitude of ascending node.
[f] Argument of perihelion.
[g] Mean anomaly at epoch 2452912.8951630 TDT (Terrestrial Dynamic Time).
[h] Non-gravitational parameter, transverse term $\mathfrak{A}_2$ computed only.

data taken in 2004 show a systematic westward deviation from the JPL ephemeris by $\sim 18''$.

We made an effort to calculate a new orbital solution to all the astrometry of 313P, and further searched for evidence of non-gravitational acceleration as might be produced by anisotropic mass loss from 313P. For this purpose, we downloaded all the available astrometric measurements from the MPC.[9] As of 2014 December 24, a total of 89 observations were obtained. We added our 30 measurements to those from the MPC, which we then fed into EXORB7[10] for orbital determination. Perturbations by planets, Pluto, and the three most massive asteroids were included in the computation with DE406. Based on initial fits, we rejected seven observations, six from the LONEOS survey of Lowell Observatory and one from the Catalina Sky Survey, since these observations displayed significant residuals (some $\geqslant 2''$) from the fit. The pure-gravity solution to the orbit, which has a root mean square (rms) uncertainty of $\pm 0\farcs577$, is listed on the left-hand side of Table 4. By experiment, we found that the inclusion of non-gravitational terms can improve the quality of the orbital fit, albeit slightly. In particular, solving for the transverse term $\mathfrak{A}_2$, as defined by Marsden et al. (1973), reduces the rms the most, to $\pm 0\farcs524$ (right-hand side of Table 4). The best-fit solution gives $\mathfrak{A}_2 = (1.77 \pm 0.49) \times 10^{-8}$ AU day^{-2}. While this is formally a 3.6σ (i.e., statistically significant) detection of non-gravitational acceleration of 313P, we prefer to consider a 5σ upper limit to the parameter $\mathfrak{A}_2 \lesssim 2.45 \times 10^{-8}$ AU day^{-2}, because the significance of the fit relies on the (arbitrary) exclusion of outlying measurements. Some attempts have been made to measure non-gravitational cometary accelerations from single apparition data (c.f. Sosa & Fernández 2011; Sekanina & Kracht 2014a, 2014b). However, Yeomans et al. (2004) have noted that finding reliable solutions for non-gravitational forces normally requires astrometry from no less than three apparitions. We anxiously await astrometry from a third orbit of 313P.

[9] http://minorplanetcenter.net/db_search
[10] EXORB7 is an orbital determination program written by A. Vitagliano, introduction at http://chemistry.unina.it/~alvitagl/solex/Exorb.html.

4. DISCUSSION

The main purpose of this paper is to check the effective scattering cross-section of 313P observed in the archival data, compared with the value derived by Jewitt et al. (2015). The apparent magnitudes of 313P, m_λ, are related to the effective scattering cross-section of materials, denoted as C_e, within some photometric aperture by the following relationship

$$C_e = \frac{\pi r_h^2 \Delta^2}{A_\lambda(\alpha)} 10^{0.4(m_{\odot,\lambda} - m_\lambda)}. \quad (2)$$

We used the compound Henyey-Greenstein (hereafter HG) model by Marcus (2007) with a pure dusty scenario so as to describe the geometric albedo as a function of phase, and chose the normalization point to be $\alpha = 0^\circ$ such that $A_\lambda(\alpha) = A_\lambda(0^\circ)\Phi(\alpha)$, where Φ is the HG model. Therefore, combining Equations (1) and (2) together, the direct relationship between $A_\lambda f\rho$ and C_e is

$$C_e = \frac{\pi\rho}{4} \frac{A_\lambda(\alpha) f\rho}{A_\lambda(0^\circ)\Phi(\alpha)}. \quad (3)$$

For simplification we assumed $A(0^\circ) = 0.05$ independent of wavelength. Uncertainties on C_e were calculated by propagation of errors. We again used the data encircled by $\rho = 5000$ km for good S/N. Figure 5 shows the cross-section as a function of time. We compared the data from 2003 to 2004 and those measured in apertures of $6''$ in radius from the 2014 apparition by Jewitt et al. (2015) as a function of the number of days past perihelion, labeled as $t - T_p$. We immediately notice that the cross-section at similar $t - T_p$ is systematically greater, by a factor of ~ 2, in 2003 data than in data from 2014. The different aperture sizes used by different authors and bandpasses cannot account for such conspicuous discrepancies. In fact the aperture of $6''$ in radius used by Jewitt et al. (2015) corresponds to a spatial size greater than ~ 6100 km, slightly larger than the size we used in this work ($\rho = 5000$ km). Evidently, the near-perihelion scattering cross-section of 313P decreased over this 11 yr period. In addition, the cross-section decreased steadily within the two months of observation in 2003, although the heliocentric distance changed by only ~ 0.1 AU.

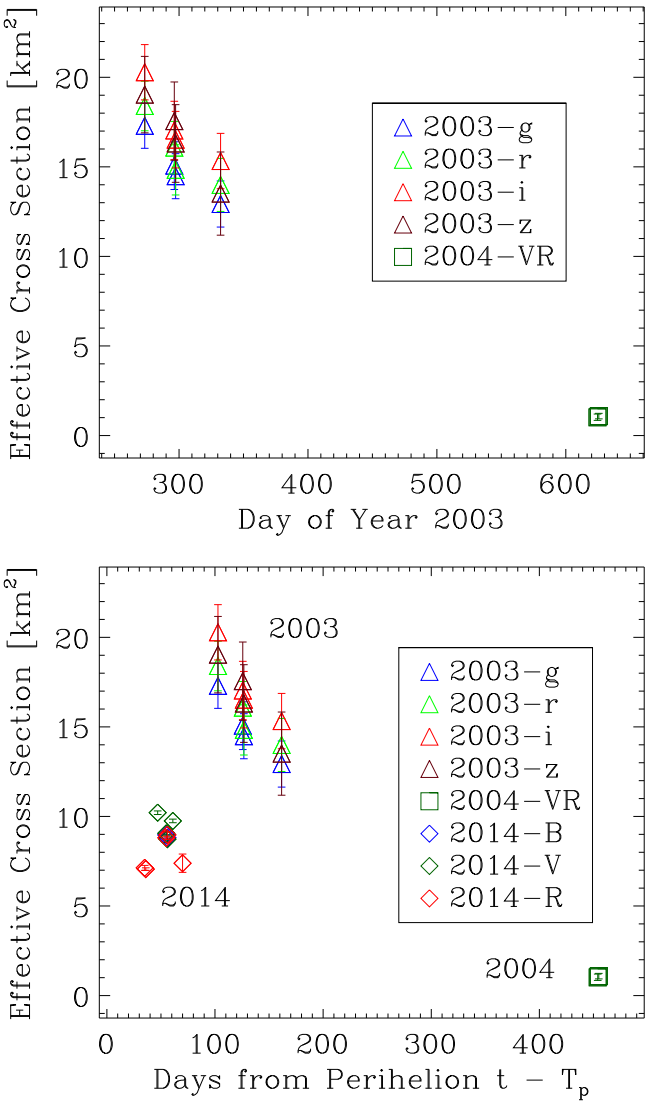

Figure 5. Scattering cross-section (km^2) as a function of time. The horizontal axis of the upper panel is Day of Year 2003, while the axis of the lower panel shows the number of days past perihelion in the corresponding apparitions. Data from 2003 and 2004 are computed by Equation (3), enclosed by a linear radius $\rho = 5000$ km. The 2014 data are extracted from Table 2 in Jewitt et al. (2014).

We estimate the mass loss rate from the photometry aperture, $\dot{M}_d$, assuming that the dust size distribution is described by a power law, $dN = Ka^{-q}da$, where dN denotes the number of dust particles having radii between a and $a + da$, and K and q are constants. The following relationship between $\dot{M}_d$ and $\dot{C}_e$ can be derived

$$\dot{M}_d = \frac{4}{3}\rho_d\left(\frac{3-q}{4-q}\right)\left(\frac{a_{\max}^{4-q} - a_{\min}^{4-q}}{a_{\max}^{3-q} - a_{\min}^{3-q}}\right)\dot{C}_e,\ q \neq 3, 4. \quad (4)$$

Without high resolution observation it is difficult to obtain an exact power law index p. We set $a_{\max} \sim 600$ and $a_{\min} \sim 25$ μm respectively, based on the syndyne and synchrone analyses, and assume a nominal $q = 3.5$. With $\rho_d = 10^3$ kg m^{-3}, the mass loss rate was estimated as $\dot{M}_d \sim 0.2$ kg s^{-1}. Altering q does not change the order of magnitude of the mass loss rate. For instance, $q = 3.9$ corresponds to $\dot{M}_d \sim 0.1$ kg s^{-1} while $q = 3.1$ gives $\dot{M}_d \sim 0.2$ kg s^{-1}. Strictly, $\dot{M}_d$ from Equation (4) is the difference between the production rate from the nucleus and the loss rate from dust escaping across the edges of the projected photometry aperture and therefore our $\dot{M}_d$ is an upper limit to the mass loss rate of the nucleus. The small value of $\dot{M}_d \lesssim 0.2$ kg s^{-1} is comparable in magnitude to the 0.2–0.4 kg s^{-1} inferred from data taken in 2014, but opposite in sign (Jewitt et al. 2015).

313P appeared completely stellar in the Subaru data from 2004 September. We calculated the radius of a sphere, r_N, equivalent to the corresponding cross-section and obtained $r_N = \sqrt{C_e/\pi} \sim 0.57 \pm 0.05$ km from 2004 September 15, and $r_N = 0.59 \pm 0.04$ km from 2004 September 16 (assuming geometric albedo 0.05). The values are the same as the $r_N \sim 0.5$ km nucleus radius reported by Jewitt et al. (2015) from *Hubble Space Telescope* observations, confirming the small size of this body.

Given the nucleus size we can also estimate a limit to the mass loss rate from the non-gravitational acceleration using Newton's law, expressed as

$$\dot{M}_d = \frac{4\pi\langle g\rangle \mathfrak{A}_2 \rho_d r_N^3}{3vk_\theta}, \quad (5)$$

where the dimensionless coefficient $\langle g\rangle = 7.6 \times 10^{-4}$ is determined by the $g(r_h)$ law in Marsden et al. (1973),[11] and v is the outflow speed of the gas. Dimensionless quantity k_θ accounts for the angular distribution of the momentum-carrying gas as it escapes the nucleus, with $k_\theta = 0$ corresponding to isotropic emission and $k_\theta = 1$ to perfectly collimated ejection. We assume $v = 0.5$ km s^{-1} and $k_\theta = 1$, to find $\dot{M}_d \lesssim 0.4$ kg s^{-1}. This value is broadly consistent with upper limits to the mass loss rate inferred above, and with gas production rate limits inferred from spectra of 313P in 2014 (Jewitt et al. 2014). Arbitrarily large limits to $\dot{M}_d$ could be obtained using values of $k_\theta < 1$. Unfortunately, this parameter is not strongly constrained by observation.

The possibility that radiation forces (e.g., the Yarkovsky effect) could account for measurable non-gravitational acceleration of 313P can be rejected. We estimate the maximum possible acceleration due to this effect by

$$a_{\rm rad} = \frac{3(1+A)F_\odot}{4\,cr_h^2\rho_d r_N} \quad (6)$$

where $F_\odot = 1361$ W m^{-2} is the solar constant at 1 AU, and $c = 3 \times 10^8$ m s^{-1} is the speed of light. Here, A is the Bond albedo, which, in the absence of constraining data, we take to be 0.05, the same as the geometric albedo. Equation (6) gives $a_{\rm rad} \sim 3.6 \times 10^{-14}$ AU day^{-2}, which is three orders of magnitude smaller than the 5σ upper limit of the measured non-gravitational acceleration $\langle g\rangle \mathfrak{A}_2 \sim 1.9 \times 10^{-11}$ AU day^{-2}.

After 133P/Elst–Pizarro and 238P/Read (c.f. Hsieh et al. 2004, 2011; Jewitt et al. 2014), 313P is only the third active main-belt asteroid to have shown mass loss in different orbits. Neither impact nor rotational instability would naturally explain this repetition of activity and so these mechanisms can be rejected. If thermal fracture or electrostatic ejection of dust were responsible for the loss of dust, then countless other asteroids in the main-belt should likewise show mass loss, but they do not. On the other hand, repetition of the activity in

[11] The quantity r_h in this paper corresponds to r in Marsden et al. (1973). We change the symbol to keep consistency.

different orbits is to be expected if the activity of 313P is driven by the sublimation of ice.

Solontoi et al. (2010) presented a visual study of active comets in SDSS data, using images taken before 2005 (Adelman-McCarthy et al. 2007), but did not include 313P. It is therefore possible that undiscovered comets lurk in archival SDSS data. 313P could also have been detected in 2008 August, as it was then at large elongation ($\gtrsim 150^\circ$) as an object of ~20 magnitude. Looking toward the future, the next perihelion of 313P will occur in 2020 April. However, the object will then be at small solar elongation ($<90^\circ$ from 2019 October to 2020 August) and repetition of the activity, if it occurs, will be more difficult to observe.

5. SUMMARY

We conducted photometric and astrometric measurements of 313P/Gibbs using archival data from 2003 and 2004. We find the following.

1. Repetition of activity 313P in separate orbits is consistent with the sublimation of ice as the driving mechanism. After 133P/Elst–Pizarro and 238P/Read, 313P is only the third active main-belt asteroid to show mass loss in different orbits.
2. The effective scattering cross-section decreased with time in 2003, even as the heliocentric distance increased by only ~0.1 AU. We estimate that the mass loss rate from the coma was $\dot{M}_d \lesssim 0.2\,\mathrm{kg\,s^{-1}}$.
3. The scattering cross-section in 2003 was about twice that in 2014, at similar heliocentric distance, suggesting a decrease in the activity on a decade timescale.
4. A syndyne and synchrone analysis showed that the activity of the target was protracted during the observations. The tail was dominated by dust grains with radii from ~25 to ~600 μm, larger than the average particle size in active comets.
5. We determine a 5σ upper limit to the transverse non-gravitational parameter, $\mathfrak{A}_2 \lesssim 2.45 \times 10^{-8}\,\mathrm{AU\,day^{-2}}$. The limit to the mass loss rate $\dot{M}_d \lesssim 0.4\,\mathrm{kg\,s^{-1}}$ estimated from the non-gravitational acceleration is consistent with the one suggested by the photometric data.
6. Subaru observations in 2004 reveal a bare nucleus about 0.5 km in radius, $A(0^\circ) = 0.05$ assumed, consistent with published observations from 2014.

We thank the anonymous referee for comments. The research used the facilities of the Canadian Astronomy Data Centre operated by the National Research Council of Canada with the support of the Canadian Space Agency. The research is partly based upon SDSS-III data, for which the funding has been provided by the Alfred P. Sloan Foundation, the Participating Institutions, the National Science Foundation, and the U.S. Department of Energy Office of Science, and is also in part based upon data collected at Subaru Telescope and obtained from SMOKA, which is operated by the Astronomy Data Center, National Astronomical Observatory of Japan. We thank Jing Li for assistance. M.-T. appreciates helpful discussions with Rainer Kracht and Matthew Knight, and suggestions from Quanzhi Ye. This work was supported, in part, by a grant to DJ from NASA's Solar System Observations program.

REFERENCES

Adelman-McCarthy, J. K., Agüeros, M. A., Allam, S. S., et al. 2007, ApJS, 172, 634
A'Hearn, M. F., Schleicher, D. G., Millis, R. L., Feldman, P. D., & Thompson, D. T. 1984, AJ, 89, 579
Ahn, C. P., Alexandroff, R., Allende Prieto, C., et al. 2012, ApJS, 203, 21
Alard, C. 2000, A&AS, 144, 363
Bohren, C. F., & Huffman, D. R. 1983, Absorption and Scattering of Light by Small Particles (New York: Wiley)
Doi, M., Tanaka, M., Fukugita, M., et al. 2010, AJ, 139, 1628
Finson, M. J., & Probstein, R. F. 1968, ApJ, 154, 327
Fulle, M. 1999, P&SS, 47, 827
Fulle, M. 2004, in Comets II, ed. M. Festou, H. U. Keller, & H. A. Weaver (Tucson, AZ: Univ. Arizona Press), 565
Gibbs, A. 2014, Central Bureau for Astronomical Telegrams, 3991
Gwyn, S. D. J., Hill, N., & Kavelaars, J. J. 2012, PASP, 124, 579
Hsieh, H. H., Jewitt, D. C., & Fernández, Y. R. 2004, AJ, 127, 2997
Hsieh, H. H., Meech, K. J., & Pittichová, J. 2011, ApJL, 736, LL18
Hsieh, H. H., Hainaut, O., Novakovic, B., et al. 2015, ApJL, 800, L16
Jester, S., Schneider, D. P., Richards, G. T., et al. 2005, AJ, 130, 873
Jewitt, D., Luu, J., & Chen, J. 1996, ApJ, 112, 1225
Jewitt, D. 2012, AJ, 143, 66
Jewitt, D., Ishiguro, M., Weaver, H., et al. 2014, AJ, 147, 117
Jewitt, D., Agarwal, J., Peixinho, N., et al. 2015, AJ, 149, 81
Marcus, J. N. 2007, ICQ, 29, 119
Marsden, B. G., Sekanina, Z., & Yeomans, D. K. 1973, AJ, 78, 211
Miyazaki, S., Komiyama, Y., Sekiguchi, M., et al. 2002, PASJ, 54, 833
Monet, D. G., Levine, S. E., Canzian, B., et al. 2003, AJ, 125, 984
Sekanina, Z., & Kracht, R. 2014, arXiv:1404.5968
Sekanina, Z., & Kracht, R. 2014, arXiv:1409.3618
Solontoi, M., Ivezić, Ž., West, A. A., et al. 2010, Icar, 205, 605
Sosa, A., & Fernández, J. A. 2011, MNRAS, 416, 767
Yeomans, D. K., Chodas, P. W., Sitarski, G., Szutowicz, S., & Królikowska, M. 2004, in Comets II, ed. M. Festou, H. U. Keller, & H. A. Weaver (Tucson, AZ: Univ. Arizona Press), 137